

Supporting Information

Highly efficient heterostructure nanorods bifunctional electrocatalyst for realizing enhanced overall water splitting at a large current density

Derun Li^a, Shixin Wu^a, Tao Jiang^a, Shuangshuang Huang^b, Zhaowu Wang^{c,d*}, Hengyi Wu^a, Guangxu Cai^a, and Feng Ren^{a,b*}

^a School of Physics and Technology, Center for Ion Beam Application Center for Electron Microscopy Hubei Key Laboratory of Nuclear Solid Physics and MOE Key Laboratory of Artificial Micro- and Nano-Structures, Wuhan University, Wuhan 430072, China

^b Center for Electron Microscopy, and MOE Key Laboratory of Artificial Micro- and Nano-Structures, Wuhan University, Wuhan 430072, China

^c School of Science, Hebei University of Technology, Tianjin 300401

^d School of Physics and Engineering, Longmen Laboratory, Henan University of Science and Technology, Luoyang 471023, China

* Corresponding authors.

E-mail: fren@whu.edu.cn (F. Ren), E-mail: wangzhaowu@haust.edu.cn (Z. Wang)

Experimental Procedures

Chemicals

NiFe foam (labeled as NFF) and Ni foam (labeled as NF) with 1.5 mm thickness were purchased from Suzhou Longshengbao Co., Ltd. (SLC, China). Potassium hydroxide (KOH), ammonium fluoride (NH₄F), and sodium sulfide (Na₂S) were purchased from Shanghai Meryer Chemical Technology Co. Ltd. (SMCTC, China). Hydrochloric acid, ethanol, and acetone were purchased from Beijing Chemical Factory. Highly purified water (resistance of 18.2 MΩ cm at 25 °C) was used for all experiments. All reagents were of analytical grade and used without further purification if not mentioned.

Materials preparation

Synthesize FeS₂/Fe-Ni₃S₂

The NFF (1.0 cm × 4.0 cm) was cleaned with deionized (DI) water, ethanol, acetone, and 3.0 M HCl by ultrasonic cleaning for 10 min, respectively. Then washed with deionized (DI) water by several times and dried in a vacuum oven. 0.1 M of Na₂S and 0.48 M of NH₄F (F48) were dissolved in 60 ml of deionized water and stirred for 10 minutes to get a clear solution. Then the mixture solution was transferred into a Teflon-lined autoclave with a volume of 100 mL, and a cleaned NFF was immersed in the above solution. The sealed autoclave was heated at 150°C for 6 h to get FeS₂/Fe-Ni₃S₂. For comparison, the experiments with different ammonium fluoride concentrations (0, 0.06, 0.12, 0.24, 0.36, and 0.6 M, denoted as F0, F6, F12, F24, F36, and F60) were carried out simultaneously.

Synthesize Ni₃S₂ and FeS₂

Ni₃S₂ electrodes were prepared through a similar process by using NF as the substrate. FeS₂ electrodes were obtained according to the reported method.¹

Synthesis of IrO₂ and Pt/C on NFF

5 mg of Pt/C was mixed with 450 μL of deionized water, 450 μL of absolute ethanol, and 20 μL of Nafion (5 wt%), and the resulting mixture was sonicated for 60 min to obtain Pt/C ink. IrO₂ ink was prepared using the same method. Then use a pipette to draw 2 μL ink each time, which was carefully dropped onto the NFF and then dried naturally at room temperature. The total ink added was 38 μL, which was dropped in 19 times for the coating. Using this method, Pt/C electrodes and IrO₂ electrodes were prepared separately.

Characterization

The X-ray diffraction (XRD) patterns were obtained from a Smart Lab 3KW with Cu Kα irradiation. The morphology of the samples was characterized by a field-emission scanning electron microscope (FE-SEM; Hitachi S-4800). Transmission electron microscope (TEM) and high-resolution transmission

electron microscope (HRTEM) images were characterized by JEM-F200 at 200 kV. The X-ray photoelectron spectroscopy (XPS) was performed on a Thermo Scientific ESCALAB 250Xi system.

Electrochemical Measurements.

All electrochemical measurements were performed on an electrochemical workstation (CHI 760E, CH Instruments Inc., Shanghai) in a typical three-electrode system. Thereinto, Hg/HgO was used as the reference electrode and a carbon rod as the counter electrode. OER performances were measured by performing linear sweep voltammetry (LSV, scan rate of 2 mV s⁻¹) in O₂ saturated 1.0 M KOH (PH = ~14) solution and HER performances were in N₂ saturated 1.0 M KOH, and all initial data were corrected against ohmic potential drop with 90% iR compensation unless otherwise noted. All the potentials reported for HER and OER was converted to the potential versus the reversible hydrogen electrode (RHE) according to the equation: E vs RHE = E vs Hg/HgO + E° Hg/HgO + 0.059pH. The effective geometric area of the electrodes remained 1 cm² and directly used as the work electrode for electrochemical characterizations. Before the LSV measurement, a number of cyclic voltammetry (CV) measures were performed at a scan of 50 mV s⁻¹ until the signals were stabilized to obtain the polarization curves. Electrochemical impedance spectroscopy (EIS) test was carried out in the range from 100 000 Hz to 0.1 Hz with 10 mV alternate current (AC) amplitude. Cyclic voltammogram (CV) measures on the different electrodes with different scan rates (50, 60, 70, 80, 90 and 100 mV s⁻¹) from 0.45 to 0.55 V vs. RHE to calculate effective electrochemical active surface area (ECSA). The long-time stability was quantified by recording a chronopotentiometry technique for three-electrode and two electrode system. The Chronopotentiometry measurement was performed to evaluate their durability at 1000 mA cm⁻² for several days. In order to maintain the pH and liquid level of the electrolyte in the CP test, a microinjector was introduced to continuously replenish deionized water.

STH Efficiency Calculation. For the photovoltaic–electrocatalysis (PV-EC) system that produces hydrogen and oxygen molecules using only solar power as the input, the solar-to-hydrogen efficiency (STH) is defined as:

$$STH = \frac{1.23V \times j_{sc} \times \eta}{P \times A}$$

Where the j_{sc} represents the operating current density of the PV-EC system, 1.23 V is corresponded to the change of Gibbs free energy of overall water splitting. η is the Faradaic efficiency, which is assumed to be 100%. A is the effective illuminated area (1 cm²), P is the power of solar illumination.

DFT calculations

All density functional theory (DFT) calculations were carried out by Vienna ab-Initio Simulation Package (VASP).² Core electrons are described by pseudopotentials generated from the projector augmented wave method,³ and valence electrons are expanded in a plane-wave basis set with an energy cutoff of 460 eV. The Perdew-Burke- Ernzerh (PBE) exchange correlation functional was used. The

surfaces are simulated by slab model with a vacuum layer of 18 Å, which is sufficiently large to exclude the influence of models in vertical direction.

For the hydrogen evolution reaction, the adsorption energy of intermediate hydrogen (ΔG_{H^*}) is the key indicator to evaluate HER catalytic activity which is calculated by following Equation:

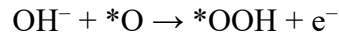
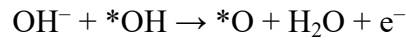
$$\Delta G_{H^*} = \Delta E_H + \Delta E_{ZPE} - T\Delta S_H$$

where ΔE_H , ΔE_{ZPE} and $T\Delta S_H$ are described the binding energy, zero-point energy change and entropy difference of hydrogen adsorption, respectively. and ΔE_H is calculated by following Equation:

$$\Delta E_H = E_{\text{surf+H}} - E_{\text{surf}} - 1/2E_{H_2}$$

where the $E_{\text{surf+H}}$ is the total energy of absorbed system, the E_{surf} and E_{H_2} are the energies of bare surface and gas phase species, respectively.

For oxygen evolution reaction in alkaline condition, the following $4e^-$ mechanism was adopted:



The “*” represents the active site when OER occurs. The “*OH”, “*O”, and “*OOH” represented the intermediate species adsorbed on the active sites. The Gibbs free energy of the adsorbed intermediates is calculated by the equation:

$$\Delta G = \Delta E + \Delta E_{ZPE} - T\Delta S.$$

Results and Discussion

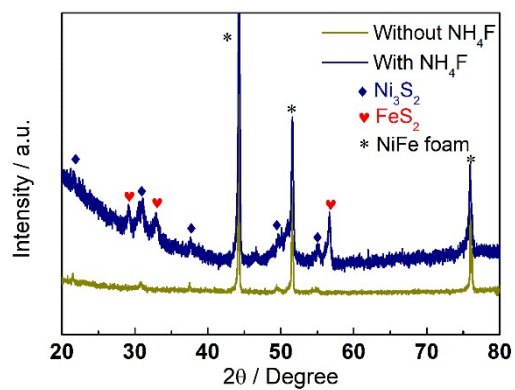


Figure S1. The XRD patterns of samples without and with NH_4F (0.48 M).

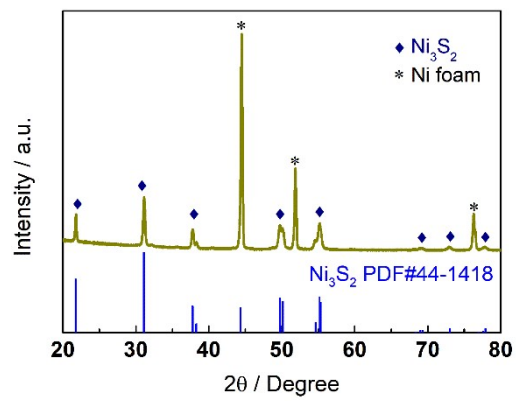


Figure S2. The XRD pattern of Ni_3S_2 .

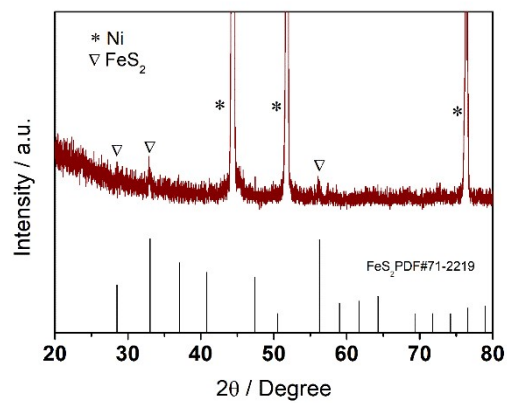


Figure S3. The XRD pattern of FeS₂/NF.

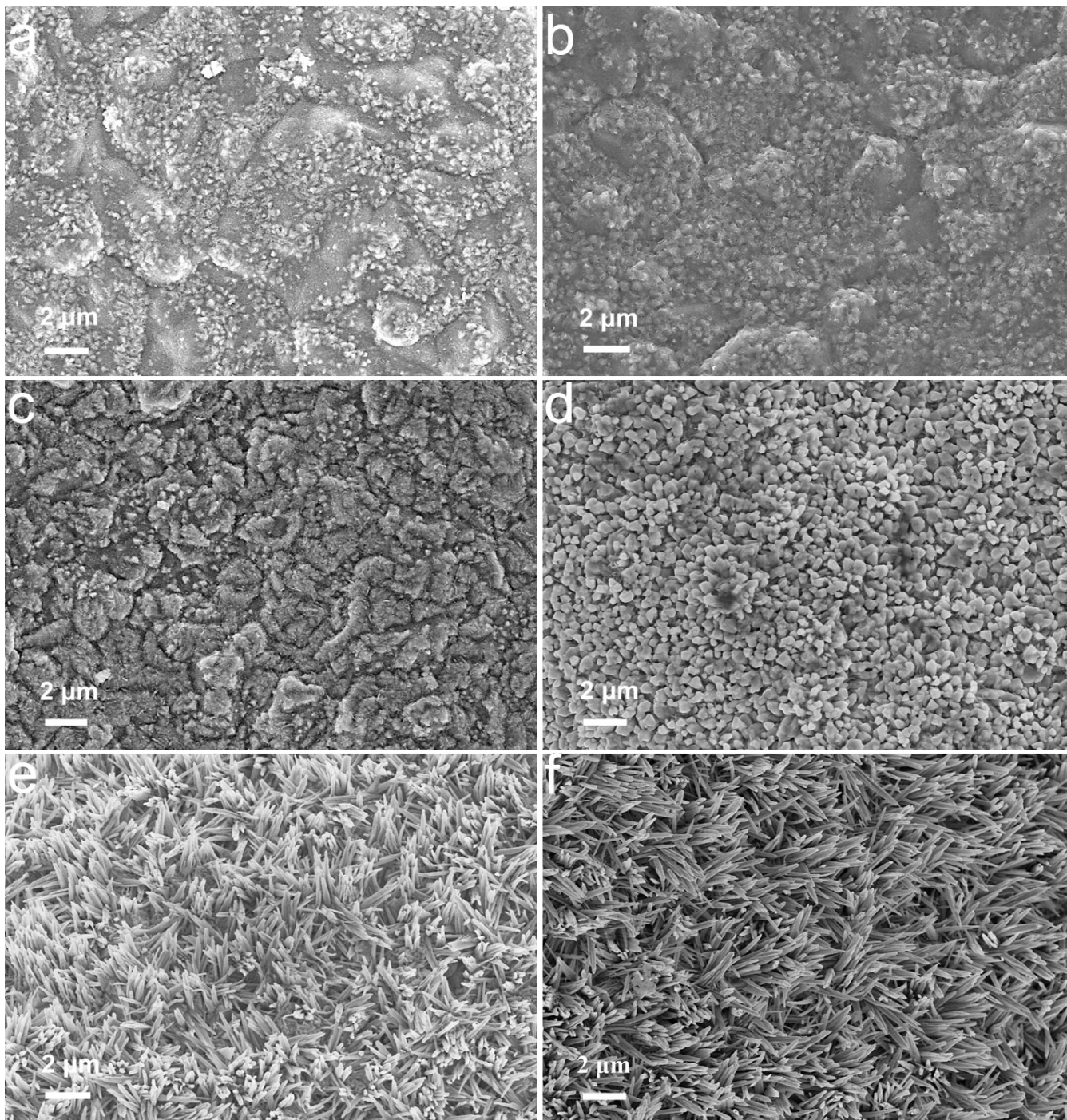


Figure S4. (a-c) The SEM images of Ni_3S_2 (F0, F6, F12) and (d-f) $\text{FeS}_2/\text{Fe-Ni}_3\text{S}_2$ (F24, F36, F60).

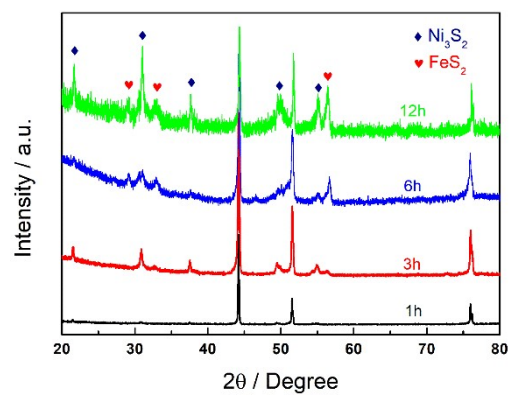


Figure S5. The XRD patterns of FeS₂/Fe-Ni₃S₂ for different preparation times (1 h, 3 h, 6 h, and 12 h).

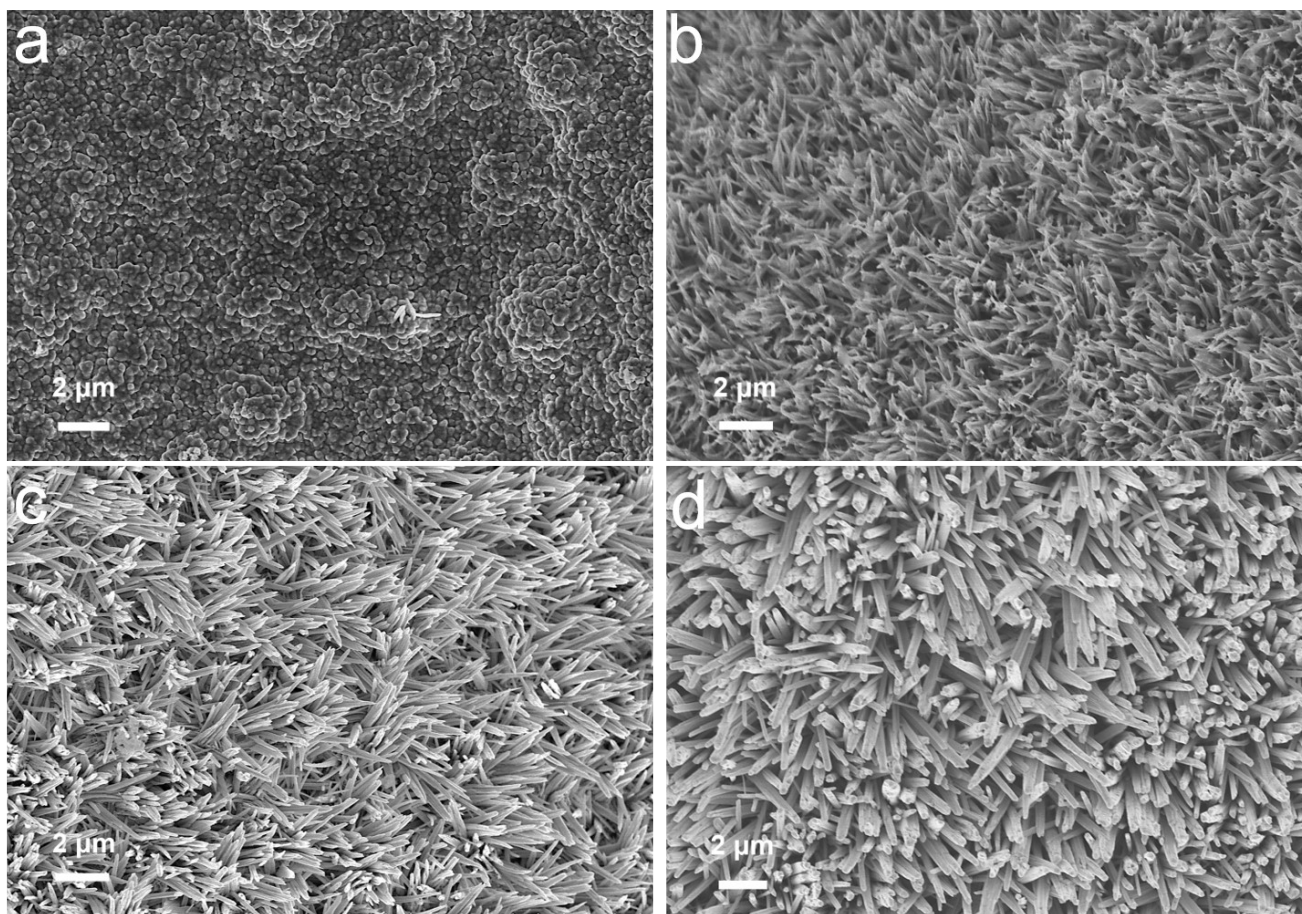


Figure S6. The SEM images of FeS₂/Fe-Ni₃S₂ for different preparation times. (a) 1 h, (b) 3 h, (c) 6 h, and (d) 12 h.

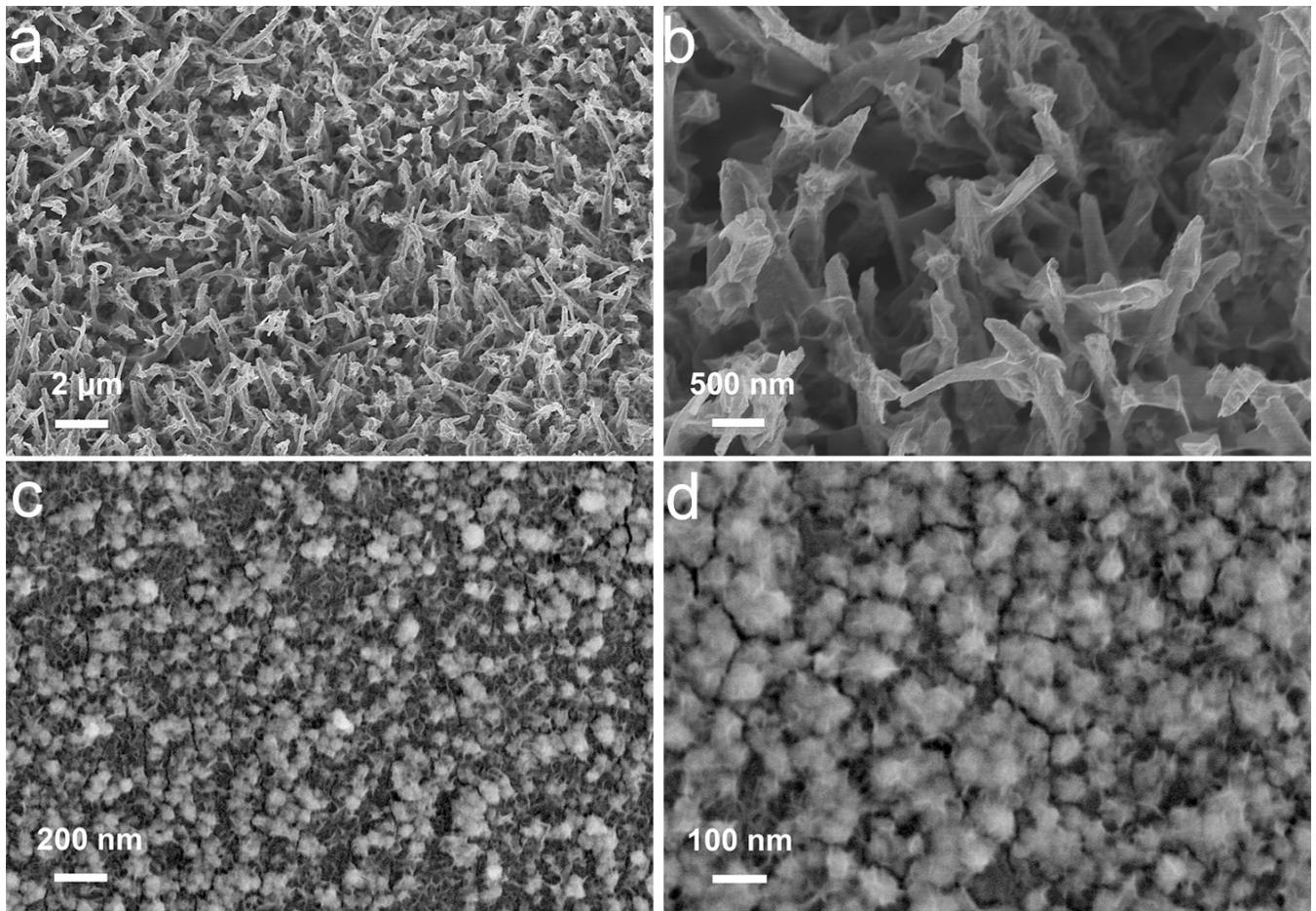


Figure S7. The SEM images of (a, b) Ni_3S_2 and (c, d) FeS_2

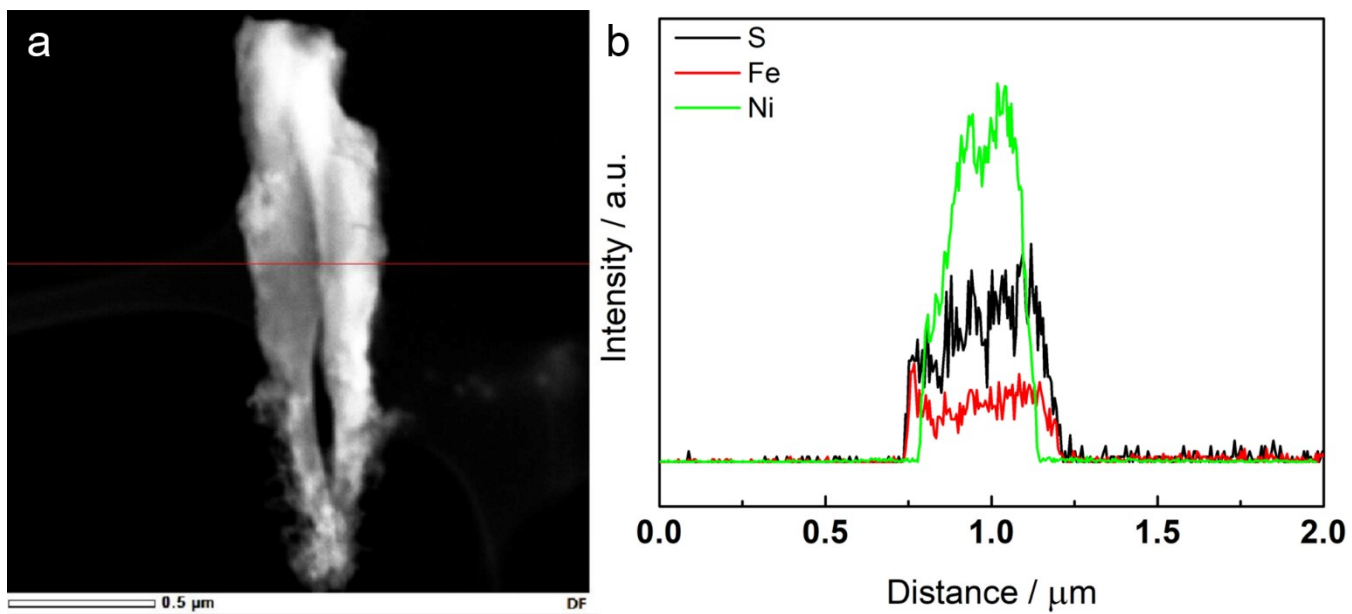


Figure S8. The TEM EDS line-scans of $\text{FeS}_2/\text{Fe-Ni}_3\text{S}_2$.

Catalyst	Electrolyte solution	Current density (j)	Overpotential	Stability test	Reference
FeS ₂ /Fe-Ni ₃ S ₂	1 M KOH	10 mA cm ⁻² 100 mA cm ⁻²	180 mV 223 mV	1000 h at 1 A cm ⁻²	This work
FeS ₂ /NiS ₂ HDSNRs	1 M KOH	50 mA cm ⁻²	280 mV	40 h at 100 mA cm ⁻²	4
FeS/Ni ₃ S ₂ @NF	1 M KOH	10 mA cm ⁻²	192 mV	/	5
IrSA/NFS	1 M KOH	10 mA cm ⁻²	230mV	350 h at 175 mA cm ⁻²	6
Ni ₃ S ₂ -NGQDs/NF	1 M KOH	10 mA cm ⁻²	218 mV	17 h at 10 mA cm ⁻²	7
a-Mo-Ni ₃ S ₂	1 M KOH	100 mA cm ⁻²	276 mV	/	8
Ni-Fe disulfide @oxyhydroxide	1 M KOH	10 mA cm ⁻²	~230 mV	50 h at 10 mA cm ⁻²	9
Fe _{11.1} %-Ni ₃ S ₂ /Ni	1 M KOH	100 mA cm ⁻²	252 mV	/	10
Ni ₃ S ₂ -Co ₉ S ₈ /NF	1 M KOH	100 mA cm ⁻²	350 mV	20 h at 100 mA cm ⁻²	11
Ni ₃ S ₂ @FeNi ₂ S ₄ @NF	1 M KOH	20 mA cm ⁻²	255 mV	24 h at 90 mA cm ⁻²	12
Ni ₃ S ₄ /NiS ₂ /FeS ₂	1 M KOH	10 mA cm ⁻²	230 mV	8 h at 10 mA cm ⁻²	13
Fe-Ni ₃ S ₂ /FeNi	1 M KOH	10 mA cm ⁻²	282 mV	9 h at 100 mA cm ⁻²	14
Zn-Ni ₃ S ₂ /NF	1 M KOH	100 mA cm ⁻²	330 mV	20 h at 50 mA cm ⁻²	15
Cu@CoS _x /CF	1 M KOH	100 mA cm ⁻²	310 mV	/	16
NiCo ₂ S ₄ NW/NF	1 M KOH	10 mA cm ⁻²	260 mV	50 h at 10 mA cm ⁻²	17
Au/Ni ₃ S ₂ /NF	1 M KOH	10 mA cm ⁻²	230 mV	60 h at 10 mA cm ⁻²	18
NiS/NF	1 M KOH	50 mA cm ⁻²	335 mV	20 h at 20 mA cm ⁻²	19
N-Ni ₃ S ₂ /NF	1 M KOH	10 mA cm ⁻²	330 mV	~3h at 50 mA cm ⁻²	20
Ni ₃ S ₂ /Fe-NiP _x /NF	1 M KOH	100 mA cm ⁻²	240 mV	200 h at 30 mA cm ⁻²	21
Ni-Ni ₃ C/CC	1 M KOH	10 mA cm ⁻²	268 mV	15 h at 20 mA cm ⁻²	22
Fe _{0.9} Ni _{2.1} S ₂ @NF	1 M KOH	100 mA cm ⁻²	252 mV	24 h at 100 mA cm ⁻²	23
NiFeCoS _x @FeNi ₃	1 M KOH	10 mA cm ⁻²	210 mV	90 h at 10 mA cm ⁻²	24

Table S1. Comparison of reported various chalcogenides for OER catalyst.

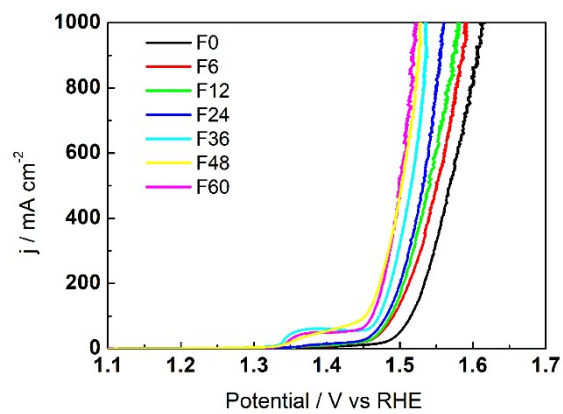


Figure S9. LSV curves of catalyst prepared with different dosages of NH_4F .

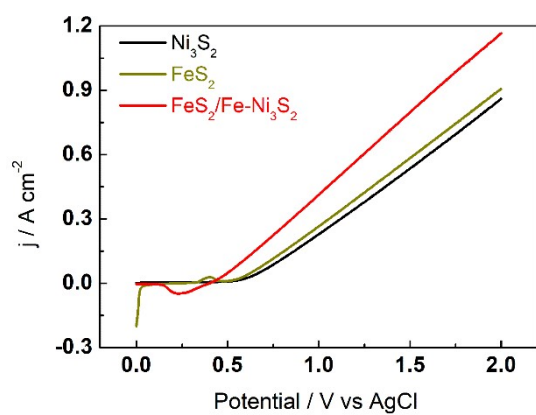


Figure S10. The LSV curves without IR correction.

Table S2. Resistance values of electron components obtained by electronic equivalent circuit simulation for OER.

	R_s (Ω)	R_{ct} (Ω)	CPE-T	CPE-P
FeS ₂ /Fe-Ni ₃ S ₂	1.291	0.37	1.225	0.612
Ni ₃ S ₂	1.017	2.08	0.04	0.92
FeS ₂	1.543	9.734	0.028	0.716

R_s is related to the series resistance. R_{ct} is the charge transfer resistance. CPE is the constant phase angle element, which represents the double-layer capacitance and inductance in the real-world situation.

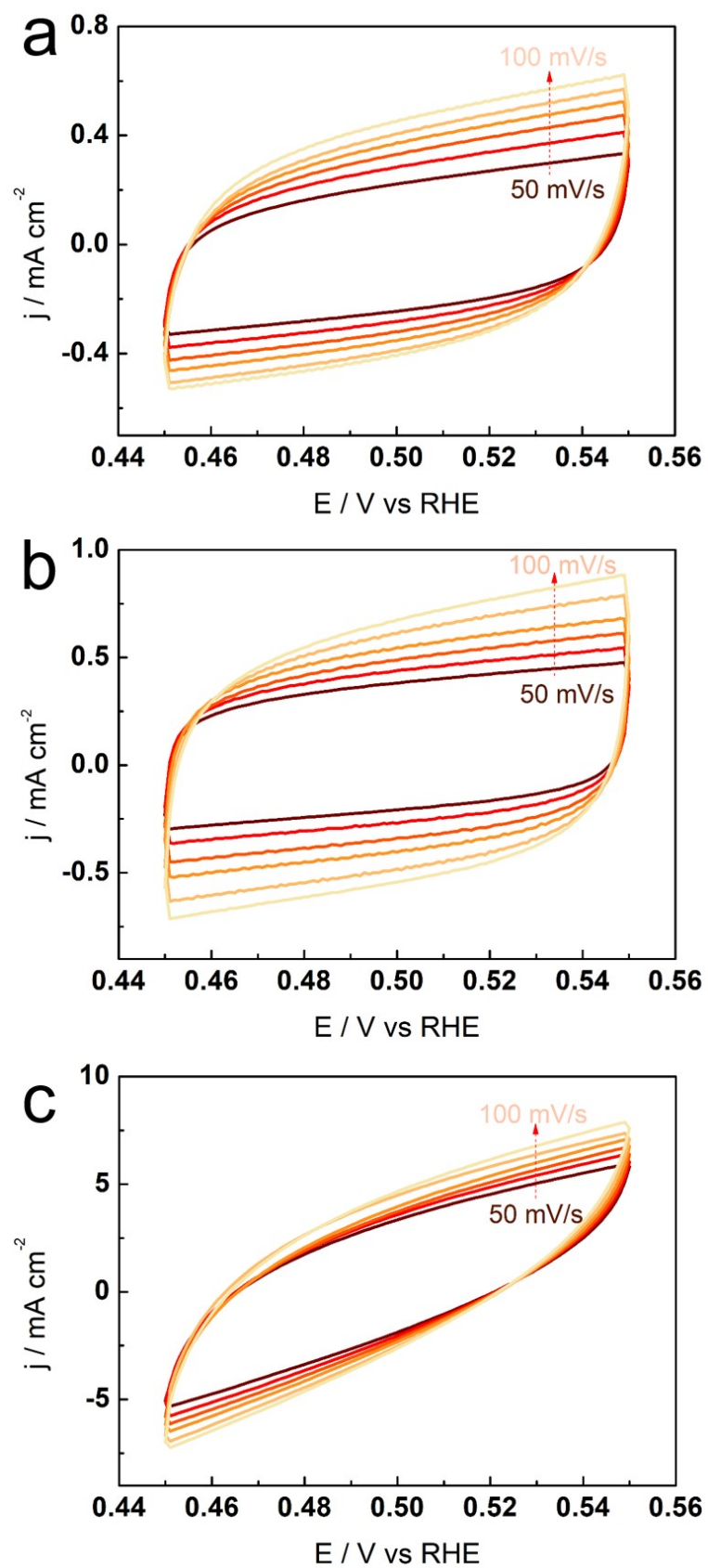


Figure S11. CV curves of (a) Ni_3S_2 , (b) FeS_2 , and (c) $\text{FeS}_2/\text{Fe-Ni}_3\text{S}_2$.

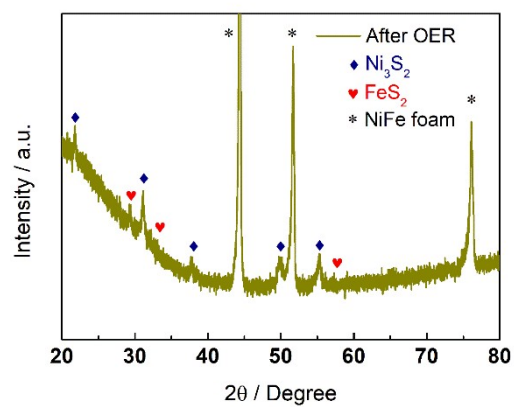


Figure S12. The XRD pattern of FeS₂/Fe-Ni₃S₂ after OER for 500 cycles.

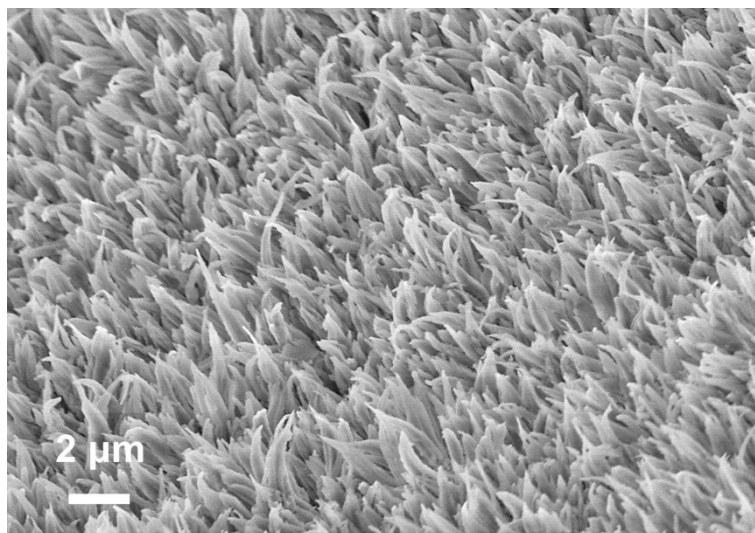


Figure S13. The SEM image of FeS₂/Fe-Ni₃S₂ after OER for 500 cycles.

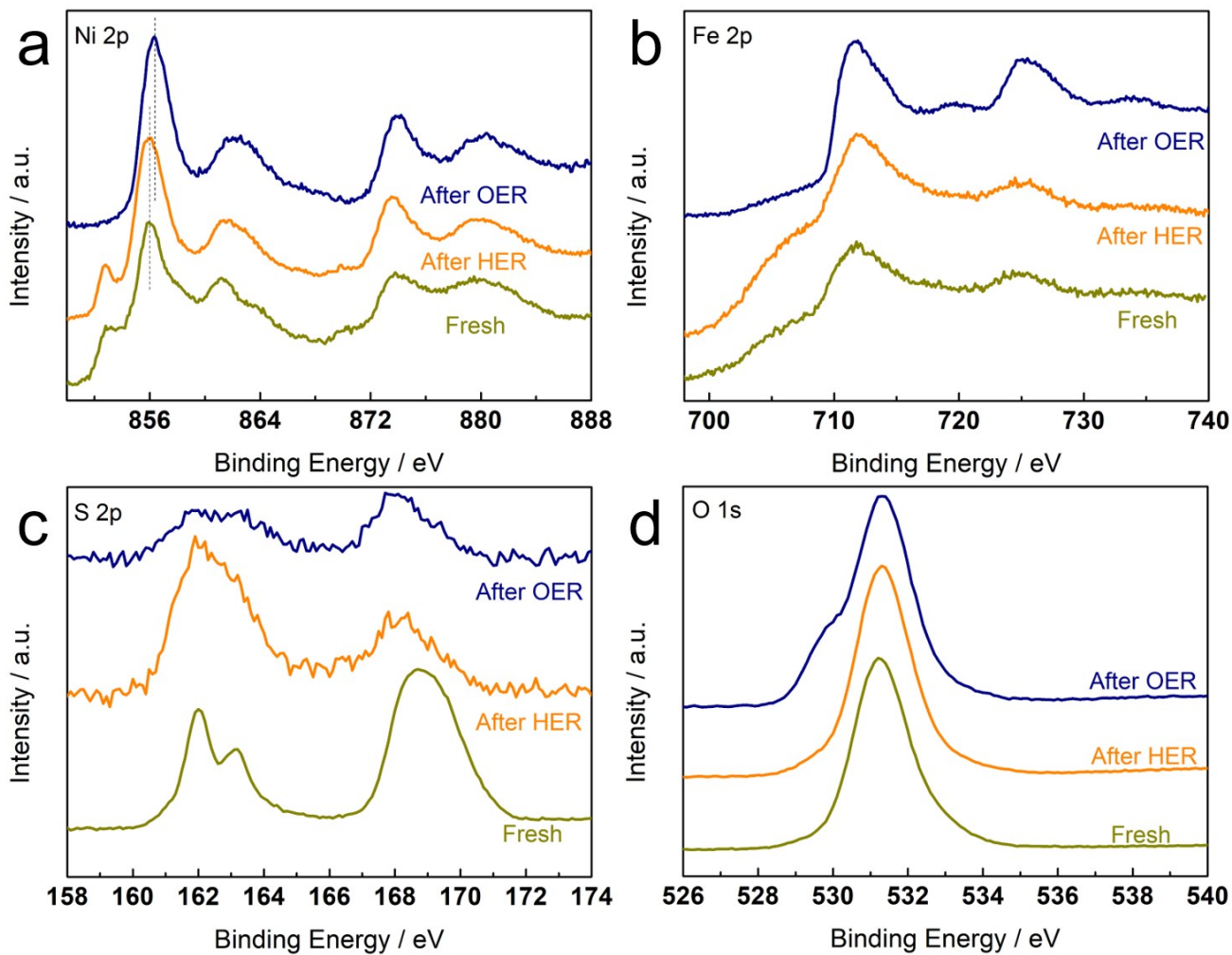


Figure S14. XPS spectrum of FeS₂/Fe-Ni₃S₂ after OER and HER for 500 cycles.

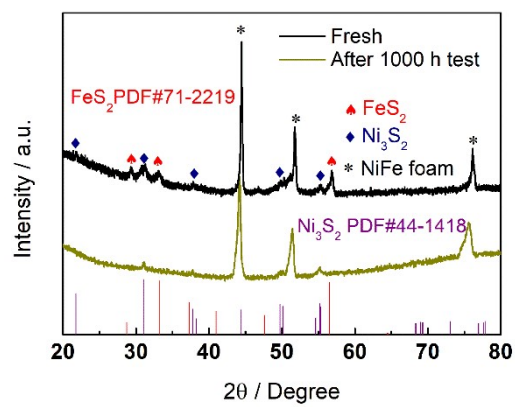


Figure S15. The XRD pattern of FeS₂/Fe-Ni₃S₂ after OER stability test at 1 A cm⁻² for 1000 h.

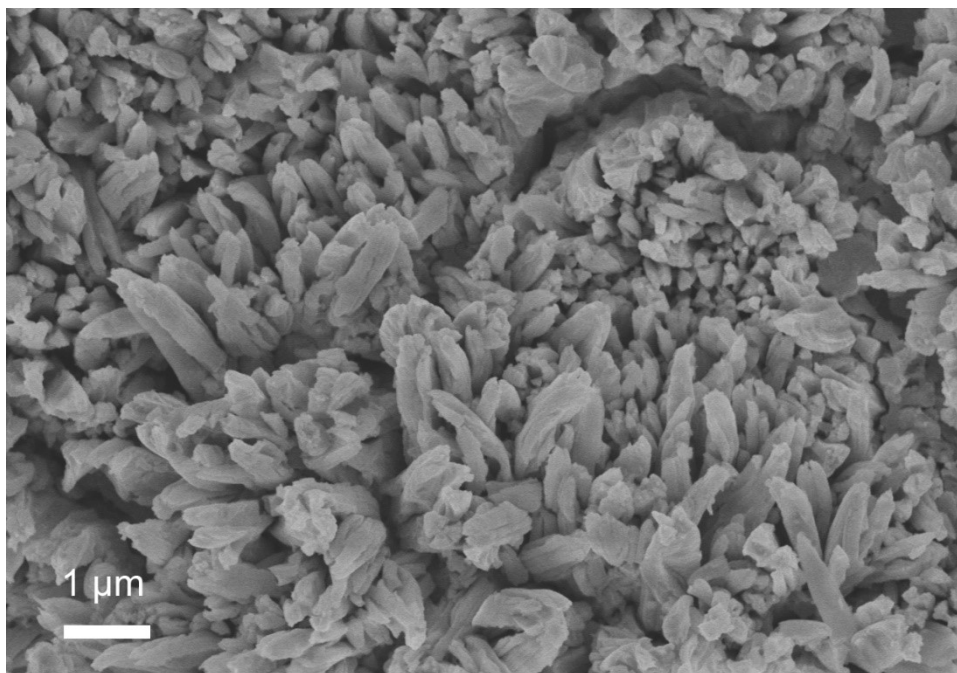


Figure S16. The SEM of FeS₂/Fe-Ni₃S₂ after OER stability test at 1 A cm⁻² for 1000 h.

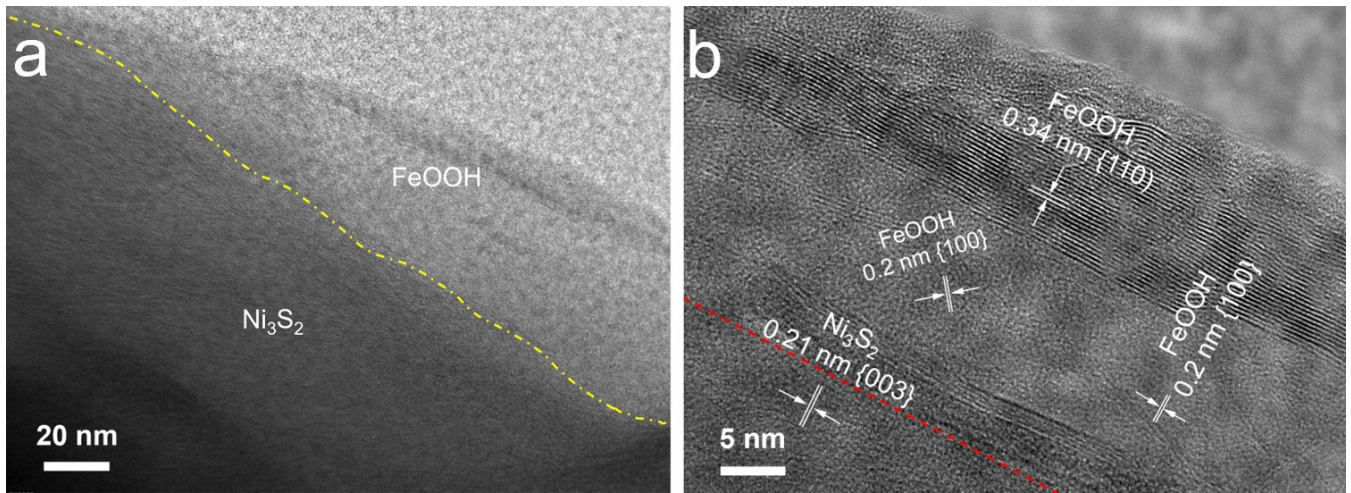


Figure S17. The HRTEM images of $\text{FeS}_2/\text{Fe-Ni}_3\text{S}_2$ after the OER stability test at 1 A cm^{-2} for 1000 h.

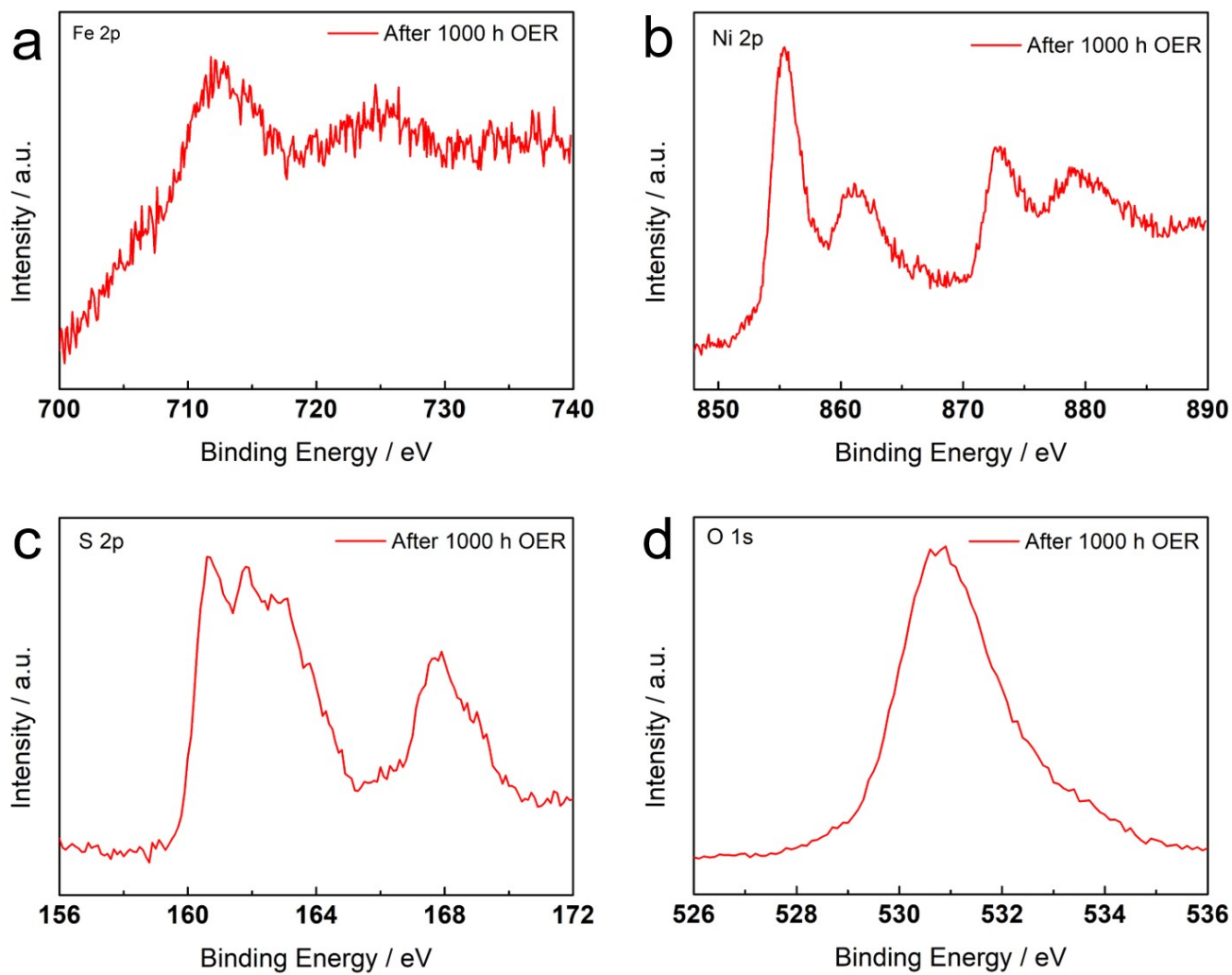


Figure S18. The XPS of FeS₂/Fe-Ni₃S₂ after OER stability test at 1 A cm⁻² for 1000 h.

Table S3. Comparison of reported various chalcogenides for HER catalyst.

Catalyst	Electrolyte solution	Current density (j)	Overpotential	Reference
FeS₂/Fe-Ni₃S₂	1 M KOH	10 mA cm ⁻² 100 mA cm ⁻²	105 mV 228 mV	This work
Ni₃S₂/NF	1 M KOH	10 mA cm ⁻²	186 mV	25
NiS/NF	1 M KOH	20 mA cm ⁻²	158 mV	19
N-Ni₃S₂/NF	1 M KOH	10 mA cm ⁻²	110 mV	20
10% VNS	1 M KOH	10 mA cm ⁻²	110 mV	26
Co₃S₄@MoS₂	1 M KOH	210 mA cm ⁻²	210 mV	27
Ni_{0.7}Fe_{0.3}S₂	1 M KOH	10 mA cm ⁻²	155 mV	28
Cu NDs/Ni₃S₂NTs	1 M KOH	100 mA cm ⁻²	128 mV	29
V-doped Ni₃S₂	1 M KOH	20 mA cm ⁻²	232 mV	30
NiCo₂S₄/Ni₃S₂	1 M KOH	10 mA cm ⁻²	119 mV	31
N-Ni₃S₂/NF	1 M KOH	10 mA cm ⁻²	155 mV	32
Ni₃S₂	1 M KOH	10 mA cm ⁻²	335 mV	33
Ni₃S₂/MnS-O	1 M KOH	10 mA cm ⁻²	116 mV	34
CoNi₂S₄/Ni₃S₂@NF	1 M KOH	10 mA cm ⁻²	171 mV	35
δ-FeOOH/Ni₃S₂/NF	1 M KOH	10 mA cm ⁻²	106 mV	36
NiWO₄/Ni₃S₂	1 M KOH	10 mA cm ⁻²	136 mV	37
Fe-Mo-S/Ni₃S₂@NF	1 M KOH	10 mA cm ⁻²	141 mV	38
Ni-FeS₂-X	1 M KOH	10 mA cm ⁻²	258 mV	39
MoS₂/FNS	1 M KOH	10 mA cm ⁻²	122 mV	40
FeS/Ni₃S₂@NF	1 M KOH	10 mA cm ⁻²	130 mV	5
FeS/NiS/NF	1 M KOH	10 mA cm ⁻²	144 mV	41

Table S4. Resistance values of electron components obtained by electronic equivalent circuit simulation for HER.

	R_s (Ω)	R_{ct} (Ω)	CPE-T	CPE-P
$\text{FeS}_2/\text{Fe-Ni}_3\text{S}_2$	1.201	0.556	0.35846	0.76683
Ni_3S_2	1.269	6.119	0.0635	0.86846
FeS_2	2.258	30.87	0.025	0.65849

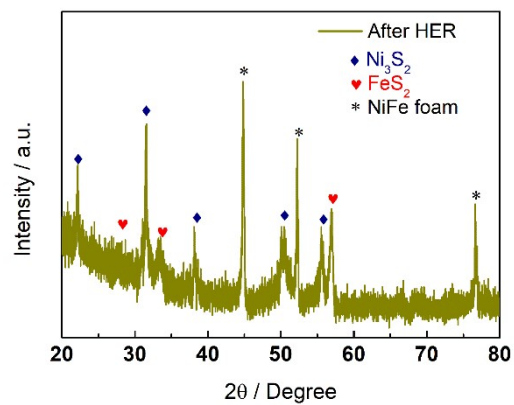


Figure S19. The XRD pattern of FeS₂/Fe-Ni₃S₂ after HER for 500 cycles.

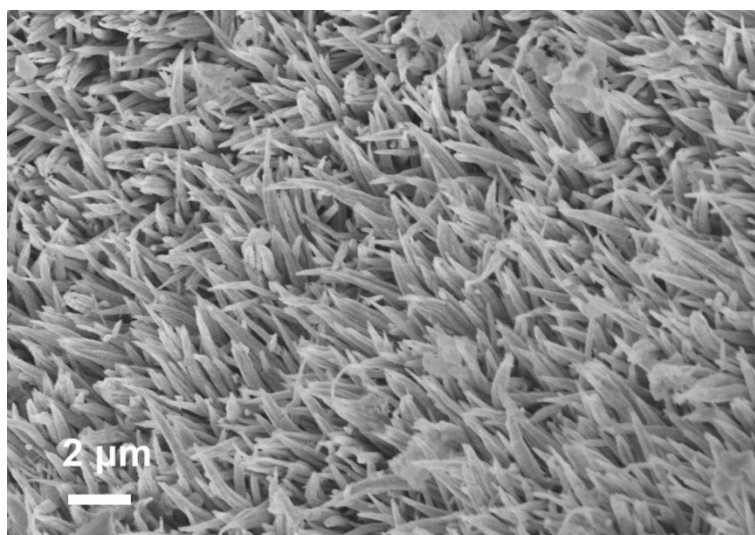


Figure S20. The SEM image of $\text{FeS}_2/\text{Fe-Ni}_3\text{S}_2$ after HER for 500 cycles.

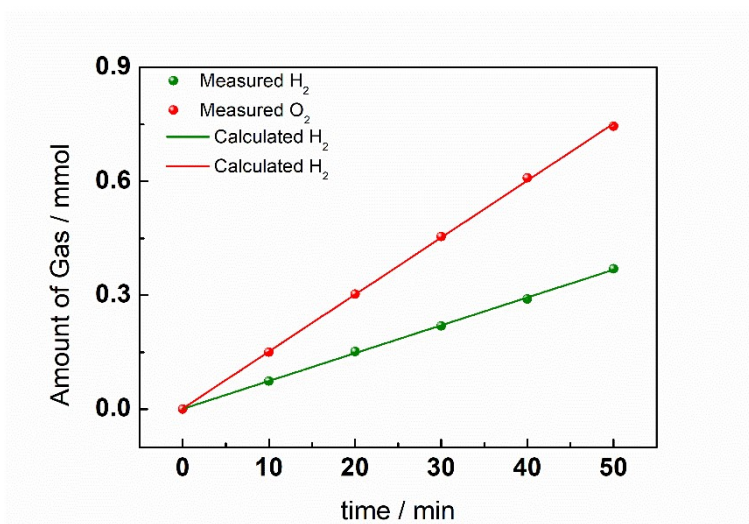


Figure S21. O₂ and H₂ production amount as a function of water splitting time powered by a constant voltage of 1.8 V.

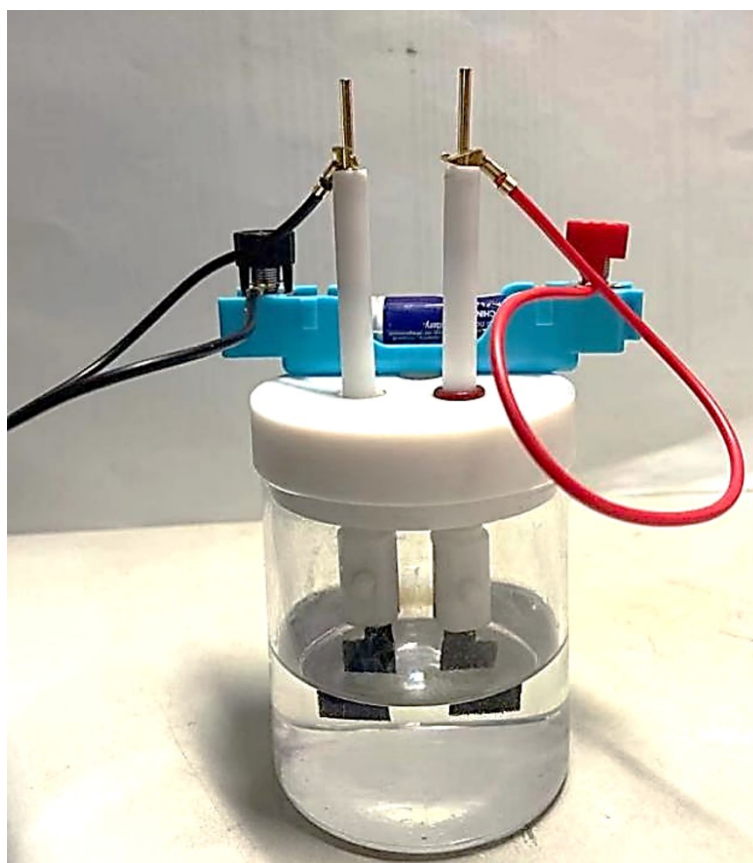


Figure S22. Photograph of water electrolyzer, assembled by $\text{FeS}_2/\text{Fe-Ni}_3\text{S}_2$ as both anode and cathode, which is powered by a single-cell AA battery of 1.5 V.

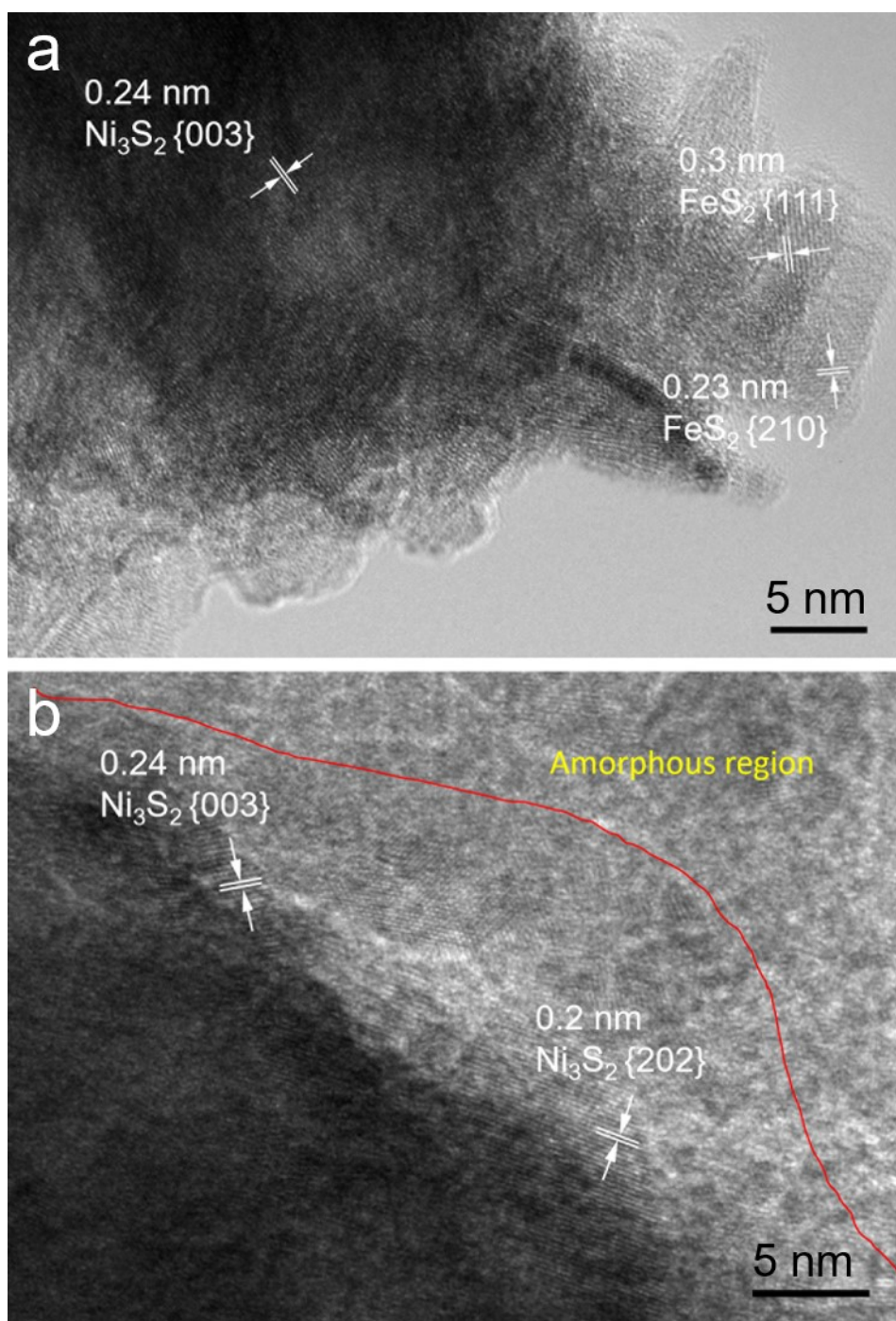


Figure S23. The HRTEM images of a) H_2 side and b) O_2 side of water-splitting after 1000 h at 1A cm^{-2} .

Table S5 Comparison of reported various chalcogenides for overall water splitting

Catalyst	Electrolyte solution	Current density (j)	Cell voltage	Stability test	Reference
FeS₂/Fe-Ni₃S₂	1 M KOH	10 mA cm ⁻² 1 A cm ⁻²	1.5 V 1.9 V	1000 h at 1 A cm ⁻²	This work
NiS/NF	1 M KOH	10 mA cm ⁻²	1.64 V	34 h at 13 mA cm ⁻²	19
Ni-Ni₃C/CC	1 M KOH	10 mA cm ⁻²	1.64 V	20 h at 20 mA cm ⁻²	22
Fe_{0.9}Ni_{2.1}S₂@NF	1 M KOH	10 mA cm ⁻²	1.51 V	100 h at 10 mA cm ⁻²	23
10% VNS	1 M KOH	10 mA cm ⁻²	1.56 V	20 h at 10 mA cm ⁻²	26
Ni_{0.7}Fe_{0.3}S₂	1 M KOH	10 mA cm ⁻²	1.625 V	~14 h at 10 mA cm ⁻²	28
CoNi₂S₄/Ni₃S₂@NF	1 M KOH	10 mA cm ⁻²	1.65 V	10 h at 10 mA cm ⁻²	35
δ-FeOOH/Ni₃S₂/NF	1 M KOH	10 mA cm ⁻²	1.525 V	24 h at 20 mA cm ⁻²	36
Ni-FeS₂-X	1 M KOH	10 mA cm ⁻²	1.55 V	22 h at 10 mA cm ⁻²	39
FeS/Ni₃S₂@NF	1 M KOH	10 mA cm ⁻²	1.51 V	50 h at 10 mA cm ⁻²	5
FeS/NiS/NF	1 M KOH	10 mA cm ⁻²	1.618 V	10 h at 10 mA cm ⁻²	41
NiS₂/FeS₂/NC	1 M KOH	10 mA cm ⁻²	1.58 V	40 h at 10 mA cm ⁻²	42
Ni₃S₂/FeNi₂S₄	1 M KOH	10 mA cm ⁻²	1.55 V	50 h at 10 mA cm ⁻²	43
NiFeCoS_x@FeNi₃	1 M KOH	10 mA cm ⁻²	1.54 V	80 h at 10 mA cm ⁻²	24
Ni₃S₄/NiS₂/FeS₂	1 M KOH	10 mA cm ⁻²	1.68 V	20 h at 10 mA cm ⁻²	13
Se-(NiCo)S/OH	1 M KOH	10 mA cm ⁻²	1.6 V	70 h at 10 mA cm ⁻²	44
NiCo₂S₄ NW/NF	1 M KOH	10 mA cm ⁻²	1.63 V	50 h at 10 mA cm ⁻²	17
Au/Ni₃S₂NF	1 M KOH	10 mA cm ⁻²	1.52 V	60 h at 10 mA cm ⁻²	18
Fe-Ni₃S₂/NF	1 M KOH	10 mA cm ⁻²	1.54 V	10 h at 10 mA cm ⁻²	45
Ni₃S₂/MnO₂	1 M KOH	10 mA cm ⁻²	1.52 V	48 h at 10 mA cm ⁻²	46
O-CoMoS	1 M KOH	10 mA cm ⁻²	1.6 V	10 h at 10 mA cm ⁻²	47

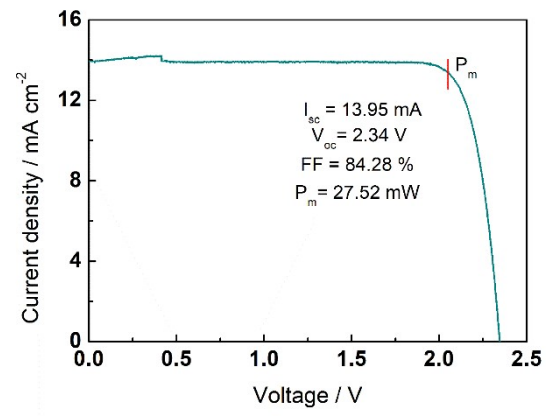


Figure S24. J–V curves of the GaInP/GaAs/Ge solar cell.

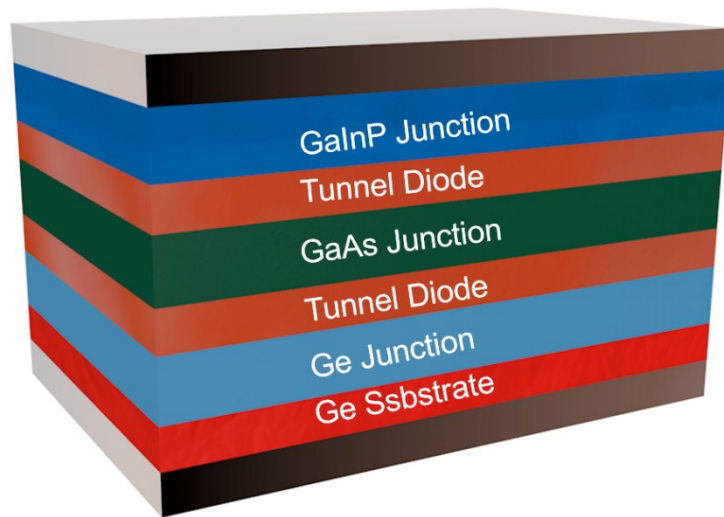


Figure S25. Structure of the GaInP/GaAs/Ge solar cell.

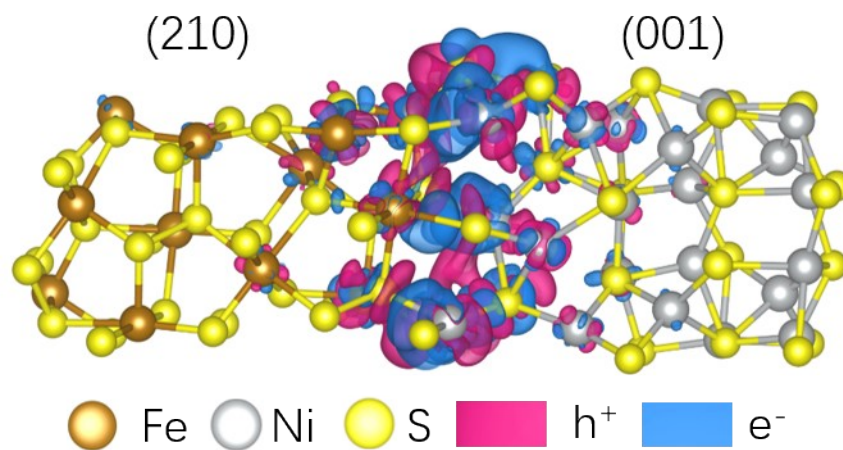


Figure S26. Optimized atomic structure of FeS₂/Ni₃S₂ heterostructure and differential charge density between FeS₂ and Ni₃S₂.

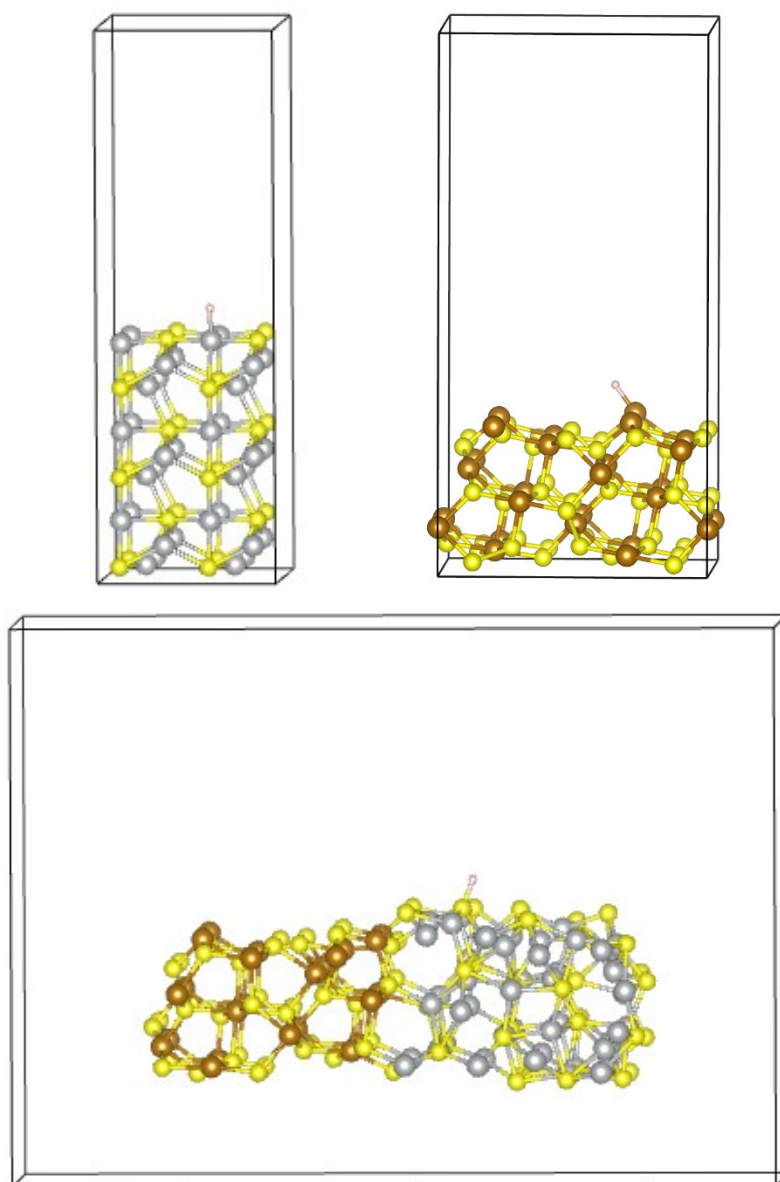


Figure S27. The configurations of hydrogen adsorption on Ni_3S_2 (001) surface, FeS_2 (210) surface, and $\text{FeS}_2/\text{Ni}_3\text{S}_2$ heterostructure.

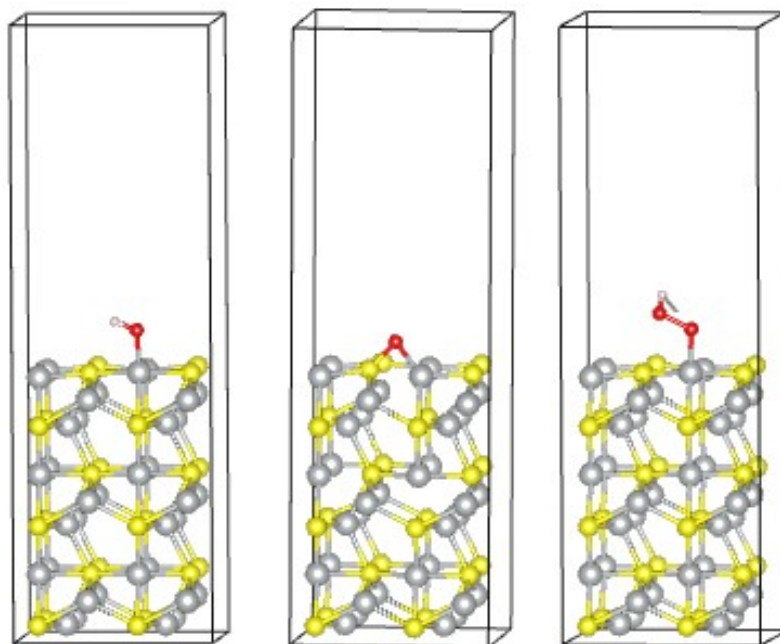


Figure S28. The configurations of the intermediates (*OH, *O, and *OOH) on the Ni₃S₂ (001) surface.

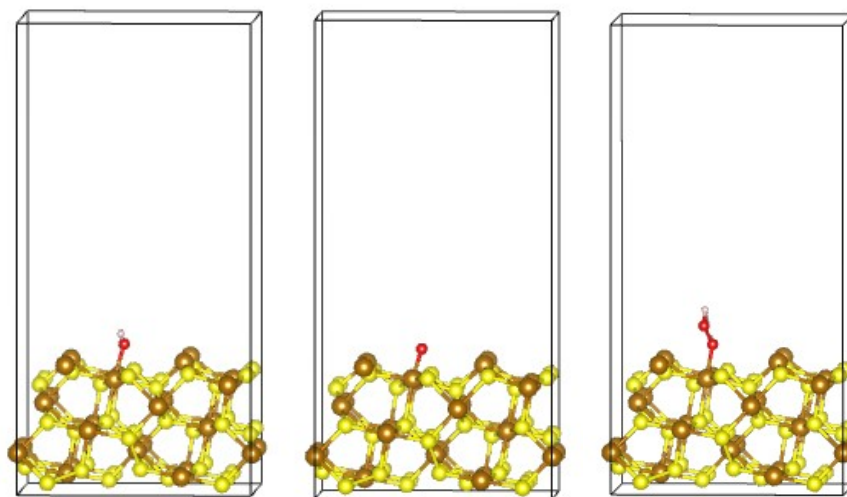


Figure S29. The configurations of the intermediates (*OH, *O, and *OOH) on the FeS₂ (210) surface.

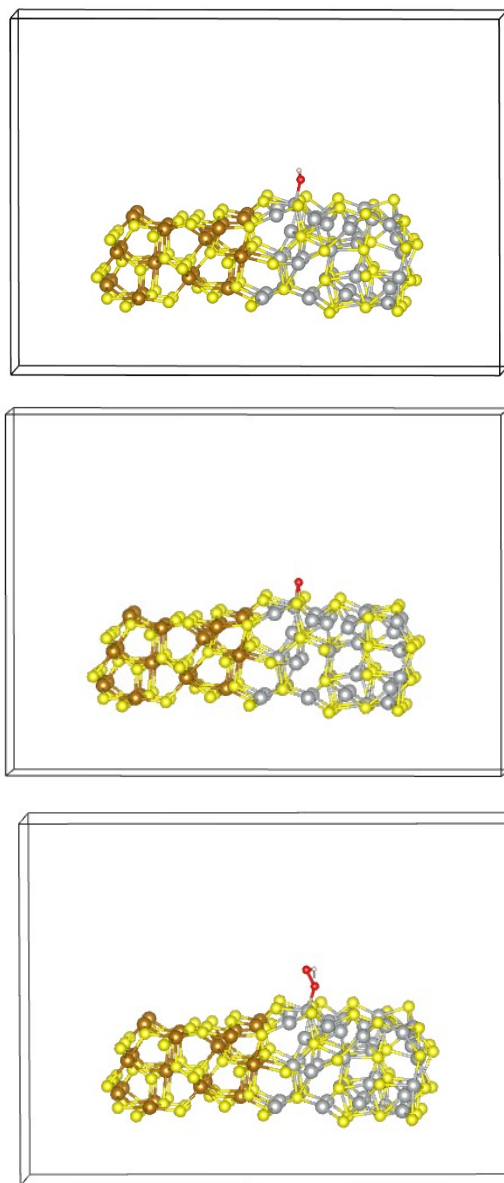


Figure S30. The configurations of the intermediates (*OH, *O, and *OOH) on the surfaces of FeS₂/Ni₃S₂ heterostructure.

Video S1. The movie shows the release of hydrogen and oxygen on the electrolyze device driven by an AA battery of 1.5 V.

Video S2. The movie shows the release of hydrogen and oxygen on the electrolyze device driven by two AA batteries in a series of 1.5 V.

Video S3. The movie shows hydrogen and oxygen release under a constant current density of 1 A cm^{-2} .

Video S4. The movie shows when the novel solar-driven water-splitting monolithic device was immersed in the electrolyte and illuminated will produce both hydrogen and oxygen.

References

1. J. Yang, H. Xuan, J. Yang, L. Meng, J. Wang, X. Liang, Y. Li and P. Han, *Appl. Surf. Sci.*, 2022, **578**, 152016.
2. G. Kresse and D. Joubert, *Phys. Rev. B*, 1999, **59**, 1758-1775.
3. G. Kresse; and J. Furthmuller., *Phys. Rev. B*, 1996, **54**, 11169-11186.
4. L. Wu, J. Li, C. Shi, Y. Li, H. Mi, L. Deng, Q. Zhang, C. He and X. Ren, *J. Mater. Chem. A*, 2022, **10**, 16627-16638.
5. H. Li, S. Yang, W. Wei, M. Zhang, Z. Jiang, Z. Yan and J. Xie, *J. Colloid Interface Sci.*, 2022, **608**, 536-548.
6. Z. Lei, W. Cai, Y. Rao, K. Wang, Y. Jiang, Y. Liu, X. Jin, J. Li, Z. Lv, S. Jiao, W. Zhang, P. Yan, S. Zhang and R. Cao, *Nat. Commun.*, 2022, **13**, 24.
7. J.-J. Lv, J. Zhao, H. Fang, L.-P. Jiang, L.-L. Li, J. Ma and J.-J. Zhu, *Small*, 2017, **13**, 1700264.
8. H. Zhang, H. Jiang, Y. Hu, P. Saha and C. Li, *Mater. Chem. Front.*, 2018, **2**, 1462-1466.
9. M. Zhou, Q. Weng, X. Zhang, X. Wang, Y. Xue, X. Zeng, Y. Bando and D. Golberg, *J. Mater. Chem. A*, 2017, **5**, 4335-4342.
10. W. Zhu, Z. Yue, W. Zhang, N. Hu, Z. Luo, M. Ren, Z. Xu, Z. Wei, Y. Suo and J. Wang, *J. Mater. Chem. A*, 2018, **6**, 4346-4353.
11. R. Zhang, L. Cheng, Z. Wang, F. Kong, Y. Tsegazab, W. Lv and W. Wang, *Appl. Surf. Sci.*, 2020, **526**, 146753.
12. Y. Yang, H. Meng, C. Kong, S. Yan, W. Ma, H. Zhu, F. Ma, C. Wang and Z. Hu, *J. Colloid Interface Sci.*, 2021, **599**, 300-312.
13. W. Wang, W. Wang, Y. Xu, X. Ren, X. Liu and Z. Li, *Appl. Surf. Sci.*, 2021, **560**, 149985.
14. C. Z. Yuan, Z. T. Sun, Y. F. Jiang, Z. K. Yang, N. Jiang, Z. W. Zhao, U. Y. Qazi, W. H. Zhang and A. W. Xu, *Small*, 2017, **13**, 1604161.
15. Q. Liu, L. Xie, Z. Liu, G. Du, A. M. Asiri and X. Sun, *Chem. Commun.*, 2017, **53**, 12446-12449.
16. Y. Liu, Q. Li, R. Si, G. D. Li, W. Li, D. P. Liu, D. Wang, L. Sun, Y. Zhang and X. Zou, *Adv. Mater.*, 2017, **29**, 1606200.
17. A. Sivanantham, P. Ganesan and S. Shanmugam, *Adv. Funct. Mater.*, 2016, **26**, 4661-4672.
18. H. Liu, J. Cheng, W. He, Y. Li, J. Mao, X. Zheng, C. Chen, C. Cui and Q. Hao, *Appl. Catal., B*, 2022, **304**, 120935.
19. W. Zhu, X. Yue, W. Zhang, S. Yu, Y. Zhang, J. Wang and J. Wang, *Chem. Commun.*, 2016, **52**, 1486-1489.
20. P. Chen, T. Zhou, M. Zhang, Y. Tong, C. Zhong, N. Zhang, L. Zhang, C. Wu and Y. Xie, *Adv. Mater.*, 2017, **29**, 1701584.
21. X. Luo, P. Ji, P. Wang, X. Tan, L. Chen and S. Mu, *Adv. Sci.*, 2022, **9**, e2104846.
22. P. Wang, R. Qin, P. Ji, Z. Pu, J. Zhu, C. Lin, Y. Zhao, H. Tang, W. Li and S. Mu, *Small*, 2020, **16**, e2001642.
23. B. Fei, Z. Chen, J. Liu, H. Xu, X. Yan, H. Qing, M. Chen and R. Wu, *Adv. Energy Mater.*, 2020, **10**, 2001963.
24. J. Shen, Q. Li, W. Zhang, Z. Cai, L. Cui, X. Liu and J. Liu, *J. Mater. Chem. A*, 2022, **10**, 5442-5451.
25. L. Li, C. Sun, B. Shang, Q. Li, J. Lei, N. Li and F. Pan, *J. Mater. Chem. A*, 2019, **7**, 18003-18011.
26. H. Liu, Q. He, H. Jiang, Y. Lin, Y. Zhang, M. Habib, S. Chen and L. Song, *ACS Nano*, 2017, **11**, 11574-11583.
27. Y. Guo, J. Tang, H. Qian, Z. Wang and Y. Yamauchi, *Chem. Mater.*, 2017, **29**, 5566-5573.
28. J. Yu, G. Cheng and W. Luo, *J. Mater. Chem. A*, 2017, **5**, 15838-15844.
29. J.-X. Feng, J.-Q. Wu, Y.-X. Tong and G.-R. Li, *J. Am. Chem. Soc.*, 2018, **140**, 610-617.
30. Y. Qu, M. Yang, J. Chai, Z. Tang, M. Shao, C. T. Kwok, M. Yang, Z. Wang, D. Chua, S. Wang, Z. Lu and H. Pan, *ACS Appl. Mater. Interfaces*, 2017, **9**, 5959-5967.
31. H. Liu, X. Ma, Y. Rao, Y. Liu, J. Liu, L. Wang and M. Wu, *ACS Appl. Mater. Interfaces*, 2018, **10**, 10890-10897.
32. T. Kou, T. Smart, B. Yao, I. Chen, D. Thota, Y. Ping and Y. Li, *Adv. Energy Mater.*, 2018, **8**, 1703538.
33. N. Jiang, Q. Tang, M. Sheng, B. You, D.-e. Jiang and Y. Sun, *Catal. Sci. Technol.*, 2016, **6**, 1077-1084.
34. Y. Zhang, J. Fu, H. Zhao, R. Jiang, F. Tian and R. Zhang, *Appl. Catal., B*, 2019, **257**, 117899.
35. W. Dai, K. Ren, Y.-a. Zhu, Y. Pan, J. Yu and T. Lu, *J. Alloys Compd.*, 2020, **844**, 156252.
36. X. Ji, C. Cheng, Z. Zang, L. Li, X. Li, Y. Cheng, X. Yang, X. Yu, Z. Lu, X. Zhang and H. Liu, *J. Mater. Chem. A*, 2020, **8**, 21199-21207.
37. S. Huang, Y. Meng, Y. Cao, F. Yao, Z. He, X. Wang, H. Pan and M. Wu, *Appl. Catal., B*, 2020, **274**, 119120.
38. Y. Zhang, H. Guo, X. Li, J. Du, W. Ren and R. Song, *Chem. Eng. J.*, 2021, **404**, 126483.
39. Z. Tan, L. Sharma, R. Kakkur, T. Meng, Y. Jiang and M. Cao, *Inorg. Chem.*, 2019, **58**, 7615-7627.
40. Y. Wu, F. Li, W. Chen, Q. Xiang, Y. Ma, H. Zhu, P. Tao, C. Song, W. Shang, T. Deng and J. Wu, *Adv. Mater.*, 2018, **30**, e1803151.
41. R. Zhang, Z. Zhu, J. Lin, K. Zhang, N. Li and C. Zhao, *Electrochim. Acta*, 2020, **332**, 135534.
42. S. Wang, P. Ning, S. Huang, W. Wang, S. Fei, Q. He, J. Zai, Y. Jiang, Z. Hu, X. Qian and Z. Chen, *J. Power Sources*, 2019, **436**, 226857.
43. Y. Wu, Y. Li, M. Yuan, H. Hao, X. San, Z. Lv, L. Xu and B. Wei, *Chem. Eng. J.*, 2022, **427**, 131944.
44. C. Hu, L. Zhang, Z. J. Zhao, A. Li, X. Chang and J. Gong, *Adv. Mater.*, 2018, **30**, e1705538.
45. G. Zhang, Y.-S. Feng, W.-T. Lu, D. He, C.-Y. Wang, Y.-K. Li, X.-Y. Wang and F.-F. Cao, *ACS Catal.*, 2018, **8**, 5431-5441.

46. Y. Xiong, L. Xu, C. Jin and Q. Sun, *Appl. Catal., B*, 2019, **254**, 329-338.
47. J. Hou, B. Zhang, Z. Li, S. Cao, Y. Sun, Y. Wu, Z. Gao and L. Sun, *ACS Catal.*, 2018, **8**, 4612-4621.

